FINAL TECHNICAL REPORT
September 1, 2006, through August 31, 2007

Project Title: **DYNAMIC MODELING OF FLUIDIZED BED FISHER-TROPSCH REACTOR**

ICCI Project Number: 06-1/ER9
Principal Investigator: Kanchan Mondal, Southern Illinois University
Other Investigators: Tomasz Wiltowski, Southern Illinois University
Project Manager: Ronald Carty, ICCI

ABSTRACT

The research aimed at developing fluidized bed models to simulate industrial fluidized bed reactors such as those used in FT synthesis, gasification, and hydrogen separation processes etc. and to aid in scaling up new processes. A two-phase, three-compartment with *n* species reaction engineering model was developed to describe behavior of fluidized-bed catalytic reactors with special emphasis to FT synthesis. It accounted for transients, axial and radial dispersion, temperature and pressure profiles, inter-phase mass and heat transfer, different hydrodynamic flow regimes, reactions with changes in molar flows and various energy options. The general model was developed such that it was able to handle multiple phases and regions. The main objective of the research work was the development of a comprehensive fluidized bed reactor model that includes stoichiometry, thermodynamics, heat and mass transfer, reaction rates and flow pattern of the different phases in the reactor, while also facilitating the analysis of dynamic behavior.

EXECUTIVE SUMMARY

The research addresses the issue of prediction of the performance of fluidized bed reactors that are being investigated in the fields of FT synthesis for coal to liquid technologies, coal gasification, hydrogen separation technologies etc. The specific application of the developed model in this project is in the area of the prediction of FT synthesis fluid bed reactor performance and the estimation of the performance of segregated dual bed fluidized reactor (with two different catalysts for synthesis and cracking) for single step production of liquid fuels with a narrow product spectrum.

Fluidized bed reactors are the reactors of choice of several important industrial processes including the Fischer-Tropsch synthesis of liquid fuels from syngas. Fluidized bed reactors are simple reactors in which a bed of catalyst is suspended by the feed gas. In spite of their simple construction, the design and scale up of these reactors are not easily accomplished primarily due to the complex physical and chemical interaction of the phases. These complex interactions yield a radial and axial distribution of catalysts, heat and concentration of the reactants and products. Most of the models currently used assume uniform distribution of the catalysts throughout the reactor. Backmixing of the reactants and products is often neglected (approaching the plug flow conditions) or is considered infinite (approaching the perfectly mixed condition). Since the majority of the reactors operate with a finite amount of backmixing, non ideal flows need to be considered. In addition, a change in gas flow rates is often observed in the reactors due to chemical kinetics in which uneven moles of reactants and products are formed (as determined by the reaction stoichiometry). Thus, a proper reactor model is required that accounts for the changes in gas flow rates and thus the gas hold-up in these reactors. Finally, the localized changes in temperature due to the reactions are often not accounted for. However, these changes have a profound effect on the reaction selectivity and thus the ultimate product distribution (as often seen in FT synthesis). Most models currently available account for these changes adopt simple assumptions (usually resulting in linearized relationships) to account for these deviations from ideality. However, most industrial processes such as the F-T synthesis require a more realistic approach. In this research a population balance, multi-component, 3- dimensional dynamic model was developed to achieve the above objective. All the variables in momentum, mass and energy were treated as time- and space- dependent. Transport phenomena principles were applied to an elemental volume with the reactor and the differential equation developed for mass and energy balance was applied along with the boundary and initial condition. The elemental volume contained 3 phases, namely gas, FT catalyst and cracking catalyst and consisted of 2 compartments in the z direction. The two compartments were essentially those of rising solids and falling solids in the bed and the associated mass transfer and heat transfer were included in the overall model.

The main objective of the research work was to lay the groundwork for the development of a comprehensive model based on dynamic population balance modeling principles in various compartments. The developed model incorporates reaction stoichiometry, thermodynamics, heat and mass transfer, reaction rates and flow pattern of the different phases in the reactor all of these features, while also facilitating the analysis of dynamic

behavior. Once the more general model has been debugged, it will be used to evaluate the performance of fluidized bed F-T reactors and its extension to other reactors such as fluidized bed gasifiers and reactive separation of hydrogen from syngas in fluidized bed reactors. In this project, unidirectional gas flow was assumed at the inlet and any radial flow was assumed to be a result of axial dispersion or convection due to temperature profiles created during the release or absorption of reaction heat. This condition was used for evaluating the model. The methodology of the dynamic model development will be extended to other types of reactors involved in FT synthesis in the future.

Task 1. Literature review

The open literature was thoroughly reviewed for existing models of fluidized bed unit processes. In addition, empirical models for predicting the hydrodynamic behavior and the various mass and heat transfer relations in different flow regimes were identified. Finally, the various reaction mechanisms suggested for FT synthesis were identified for development of the micro-kinetic model.

Task 2. Data Collection

The literature was thoroughly reviewed for collection of data in FT processes conducted in fluid bed reactors. This data was used for model validation and parameter estimation.

Task 3. Conceptual Design of Model Reactor

A conceptual model of the fluid bed reactor was developed and the dimensions and geometry were defined.

Task 4. Dynamic Population Balance Model Development

A population balance based dynamic model was formulated. The fluidized-bed model described the transfer and conversion of the mass under the action of gravity, fluid flow and reaction. There are two parts of the model, i.e., energy and mass balancing. Mass balancing throughout the system was achieved by dividing the fluidized-bed reactor into zones that have specific characteristics associated with physical and operating parameters. In one set of modeled, each physical zone was then divided up into 3 compartments - solid-gas (SG), solid (S) and gas (G) phases. In a second set of models, each elemental volume was divided into 2 compartments in the z direction, namely one compartment with falling solids and the second with rising solids. Axial and lateral mixing of solids was accounted for using compartmental modeling. Axial dispersion was also included in the model. Mass balance in each of the three compartments in each zone was used in conjunction with the overall mass balance. Species mass balance in each of the 3 phases was also used. Chemical reaction was assumed to occur only on the solid surface. Energy balance equations (incorporating enthalpy of phase change) were employed to predict the temperature distributions. The above conservation equations were combined with holdup and space time. The local pressure was calculated as the summation of the reactor inlet pressure and the static head pressure. The change in the gas flow rate is

calculated from the overall gas mass balance equation. The total gas holdup is dependent on the superficial gas velocity and the physical properties of the system. The model was initially developed in rectangular coordinates for simplicity, and was then used to develop a model in cylindrical coordinate system.

Task 5. Sensitivity Analysis of Parameter

Sensitivity analysis of the parameters was conducted using known values of several coefficients. This analysis identified the most significant parameters and the validity of some of the assumptions.

Task 6. Model Validation, Prediction and Extension

The model was validated using the data collected from the literature. However, due to lack of extensive data on fluidized bed FT synthesis, this task could not be completed with the rigor required of such models and for parameter estimation. The data obtained from this task provided information for designing a fluidized bed reactor for FT synthesis with high selectivity and predicting the behavior after scale-up. The behavior and the expected product spectrum in such a reactor for various configurations and feed and operating conditions were evaluated. The model will be extended to the dual bed fluidized bed reactor wherein both synthesis and cracking is achieved in the same reactor. The behavior and the expected product spectrum in such a reactor for various configurations and feed and operating conditions will be evaluated.

Task 7. Reporting

This task provides for the work associated with the technical direction, scheduling, cost control, and reporting on the project.

OBJECTIVES

The main objective of the research work was the development of a comprehensive model based on dynamic population balance modeling principles in various compartments. The model developed incorporates reaction stoichiometry, thermodynamics, heat and mass transfer, reaction rates and flow pattern of the different phases in the reactor all of these features, while also facilitating the analysis of dynamic behavior. This model also includes most existing fluid bed reactor models as special cases, allowing clear connections to be established among the models and showing the significance and implications of each simplifying assumption. The objective of this research was set the foundation and the path that would lead to a more systematic approach to fluidized-bed reactor modeling.

The scope of this research was to develop a dynamic population balance model that can be used to simulate catalytic reactions in fluidized bed reactors. The ultimate aim of the research was to develop a multiphase, multicomponent reaction engineering model to investigate the dynamic and steady state behavior of fluidized-bed simultaneous FT synthesis and catalytic cracking. The model accounts for transients, axial and radial dispersion, temperature and pressure profiles, inter-phase mass and heat transfer, different hydrodynamic flow regimes, reactions with changes in molar flows and various energy options. It is also able to handle multiple phases and regions (dense phase, dilute phase, etc). Successful development of the complete model will result in enhanced ability to describe reacting systems using fewer assumptions than other models in the literature. Although the scope of this exploratory research is limited to FT synthesis, the general form of the model itself would be applicable in a wide variety of applications. For example, successful completion of the preliminary model development and validation phase will lead to the modeling of the fluidized bed FT reactor in which two different catalysts (synthesis and cracking) can be used such that there are two layers. The first catalyst (with higher density, will form the lower bed) will catalyze the FT reaction while the second catalyst with lower density (upper layer of the fluidized bed) will catalyze the wax cracking reaction. In the current model, the distinction was not made between the two catalysts.

TASKS

Task 1. Literature review

The open literature was thoroughly reviewed for existing models of fluidized bed unit processes. In addition, empirical models for predicting the hydrodynamic behavior and the various mass and heat transfer relations in different flow regimes was also identified. Finally, the various reaction mechanisms suggested for FT synthesis was identified for development of the micro-kinetic model.

Task 2. Data Collection

The literature was thoroughly reviewed for collection of data in FT processes conducted in fluid bed reactors. This data was used for model validation and parameter estimation.

Task 3. Conceptual Design of Model Reactor

A conceptual model of the fluid bed reactor was developed and the dimensions and geometry were defined.

Task 4. Dynamic Population Balance Model Development

A population balance based dynamic model was formulated.

Task 5. Sensitivity Analysis of Parameter

Sensitivity analysis of the parameters was conducted using known values of several coefficients. This analysis identified the most significant parameters and the validity of some of the assumptions.

Task 6. Model Validation, Prediction and Extension

The model was validated using the data collected from the literature. However, due to lack of extensive data on fluidized bed FT synthesis, this task could not be completed rigorously.

Task 7. Reporting

This task provides for the work associated with the technical direction, scheduling, cost control, and reporting on the project.

INTRODUCTION AND BACKGROUND

A typical fluidized-bed reactor employs gas (sometimes referred to as elutriation or fluidization medium) introduced at the bottom of the device to suspend particles. The feed gas enters with the fluidization medium. Manipulation of the gas holdup and space time allows the appropriate residence time for conversion. The FT reaction is a highly exothermic one and therefore, gas–solid fluidized-beds, with their excellent heat transfer and temperature equalization characteristics are very attractive. The use of small catalyst particles, e.g., of about 100 μm diameter, ensures freedom from pore diffusion limitations. However, a serious issue is the possibility that heavy product deposits on the catalyst, causing particles to agglomerate, and thus, hampering fluidization. To avoid this problem, commercial gas–solid fluidized FT processes operate at relatively high temperature and moderate pressure, producing a relatively light product due to low chain growth probability (α) under these conditions. The condition for Anderson Schulz Flory distribution (ASF) is that α must be less than 0.71 rules out the possibility of applying

gas–solid ASF fluidized-beds for FT processes that produce much heavier products than gasoline. Even when low operating pressures and relatively high temperatures are adopted, the heavier tail of a high α product will inevitably condense on the catalyst particles.

The fluidized bed reactor has a lot of advantages: excellent gas-solid contacting, no hot spots even with very exothermic reactions, good gas-to-particle and bed-to-wall heat transfer and the ease of solids handling which is particularly important if the catalyst is quickly ageing. However, the list of disadvantages is as long: broad residence time distribution of the gas due to dispersion and gas-bypass in the form of bubbles, broad residence time distribution of solids due to intense mixing, erosion of bed internals and the attrition of the catalyst particles. A particular disadvantage of the fluidized bed reactor is its difficult scale-up. The historical experience with the fluidized catalytic cracking (FCC) process is that in the early 40's of the last century this process was successfully scaled up from a 5 cm dia. pilot-scale unit to a 4.5 m dia. bed in the production unit. On the other hand, around 1950 the scale up of the Fischer-Tropsch synthesis in the fluidized bed failed completely. Modern process design should be able to avoid such disasters by making use of modeling and simulation tools. However, a modeling tool which is really helpful in planning and designing of an industrial fluidized bed reactor has to fulfill a lot of requirements. It should be able to describe the influence of the several changes which are typical for the scale-up process, for example enlargement of bed diameter, bed height and fluidizing velocity, changes of gas distributor design, introduction of in-bed heat exchanger tubes and baffles. In the present work, a modeling approach is presented which is able to handle the most important aspects of industrial fluidized bed reactors. After development and validation of the model, a model with the particular focus to describe the relationship between catalyst attrition, solids recovery in the reactor system and chemical performance of the fluidized bed reactor will be developed. The competing effects of attrition of the catalyst particles and efficiency of the solids recovery lead to the establishment of a catalyst particle size distribution in the bed inventory which in turn influences via the hydrodynamic characteristics of the fluidized bed the performance of the chemical reactor.

Several models are available for the simulation of FT synthesis in bubble cap reactors. In addition, several models for gas phase reactions in fixed bed reactors are also available. However, there is limited data and modeling efforts on fluidized bed catalytic reactors and even less on the fluidized bed FT synthesis reactors. This research aims at bridging the gap and developing models for fluid bed reactors in general that can be utilized for the FT synthesis in such reactors.

The FT synthesis reaction scheme is shown below.

$$CO + 2H_2 \rightarrow -CH_2- + H_2O$$

The Yates and Satterfield kinetics usually used to describe the kinetics of the above reaction.

$$-R_{CO} = \frac{a p_{H_2} p_{CO}}{(1 + b p_{CO})^2}$$

where, R_{CO} is the consumption rate of CO expressed in mole CO per kilogram of catalyst per second, and, a and b are constants (published in literature for various catalysts) dependent only on temperature of the process. A simpler first order kinetics, has also been suggested and used in various other reactor models for FT synthesis. However, the Yates–Satterfield kinetics is more realistic when operating at high syngas conversion above 60% and when the H_2/CO feed ratio is 2 (close to the stoichiometric ratio). At these conditions H_2 is not the limiting species. It is must be noted that the Yates–Satterfield kinetics were determined for a narrow temperature range of 220–240^{o}C, and hydrocarbon selectivity was not included in their model. To describe the catalyst selectivity, the Anderson–Schulz–Flory for the carbon number distribution is usually chosen. Considering that most of the hydrocarbon products are paraffins, the mole fraction of each species C_nH_{2n+2} is obtained by $x_n = (1-\alpha_{ASF})\,\alpha_{ASF,}$ where α_{ASF} is the probability factor of hydrocarbon chain growth. The higher the α_{ASF} factor, the higher is the fraction of heavy paraffins. An in depth literature review was conducted to collect data on several rate forms for syngas conversion and the rates of individual hydrocarbon formation.

EXPERIMENTAL PROCEDURES

Task 1. Literature review

The open literature was thoroughly reviewed for existing models of fluidized bed unit processes. In addition, empirical models for predicting the hydrodynamic behavior and the various mass and heat transfer relations in different flow regimes were also identified. Finally, the various reaction mechanisms suggested for FT synthesis were identified for development of the micro-kinetic model.

Task 2. Data Collection

The literature was thoroughly reviewed for collection of data in FT processes conducted in fluid bed reactors. This data was used for model validation and parameter estimation.

Task 3. Conceptual Design of Model Reactor

A conceptual model of the fluid bed reactor was developed and the dimensions and geometry were defined.

Task 4. Dynamic Population Balance Model Development

A population balance based dynamic model was formulated. The fluidized-bed model described the transfer and conversion of the mass under the action of gravity, fluid flow and reaction. There are two parts of the model, i.e., energy and mass balancing. Mass balancing throughout the system was achieved by dividing the fluidized-bed reactor into

zones that have specific characteristics associated with physical and operating parameters. In one set of modeled, each physical zone was then divided up into 3 compartments - solid-gas (SG), solid (S) and gas (G) phases. In a second set of models, each elemental volume was divided into 2 compartments in the z direction, namely one compartment with falling solids and the second with rising solids. Axial and lateral mixing of solids was accounted for using compartmental modeling. Axial dispersion was also included in the model. Mass balance in each of the three compartments in each zone was used in conjunction with the overall mass balance. Species mass balance in each of the 3 phases was also used. Chemical reaction was assumed to occur only on the solid surface. Energy balance equations (incorporating enthalpy of phase change) were employed to predict the temperature distributions. The above conservation equations were combined with holdup and space time. The local pressure was calculated as the summation of the reactor inlet pressure and the static head pressure. The change in the gas flow rate is calculated from the overall gas mass balance equation. The total gas holdup is dependent on the superficial gas velocity and the physical properties of the system. The model was initially be developed in rectangular coordinates for simplicity (provided in the Interim Report), and was then used to develop the model in cylindrical coordinate system.

Task 5. Sensitivity Analysis of Parameter

After debugging the model, sensitivity analysis of the parameters were conducted using know known values of several coefficients. This analysis identified the most significant parameters and the validity of some of the assumptions.

Task 6. Model Validation, Prediction and Extension

The model was validated using the data collected from the literature. However, due to limited data available on FT synthesis in fluid bed reactors, this task could not be completed effectively. The data obtained from this task will provide information for designing a fluidized bed reactor for FT synthesis with high selectivity and predicting the behavior after scale-up. The behavior and the expected product spectrum in such a reactor for various configurations and feed and operating conditions were evaluated. The model was extended to the dual bed fluidized bed reactor wherein both synthesis and cracking is achieved in the same reactor.

Task 7. Reporting

This task provides for the work associated with the technical direction, scheduling, cost control, and reporting on the project. An interim report and a comprehensive final report has been already prepared and submitted.

RESULTS AND DISCUSSION

Task 1. Literature review

The extant literature was thoroughly searched for models used to describe FT synthesis in fluid bed reactors. However, such models were not available in literature. However, multi-component fluidized bed models in rudimentary forms were available. The main accomplishment in this task was the search on the available kinetic models for FT reactions. The summary of that search is provided below.

Kinetics

The comprehensive modeling of fluidized bed reactors requires the consideration of several phenomena. One of the considerations is the generation or consumption of species by chemical reactions. A major problem in mathematically describing the FT synthesis is the complexity of the reaction mechanism and the large number of species involved. A simplistic approach to the mechanism of Fisher Tropsch synthesis is shown below.

Initiation

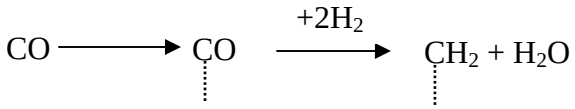

Chain Propagation

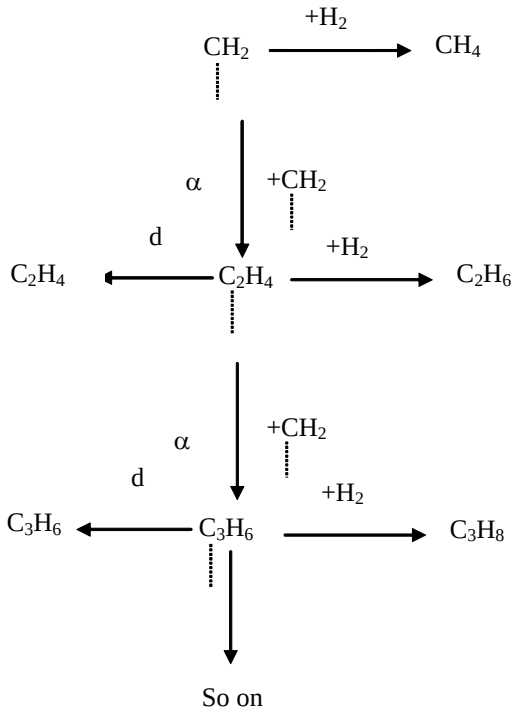

Assuming the formation of alkanes, the following stoichiometry is true.

$nCO + (2n+1)\,H_2 \rightarrow CH_3(-CH_2-)_{n-2}CH_3 + nH_2O$

In the event alkenes are produced, the following stoichiometry is assumed.

$nCO + 2nH_2 \rightarrow (CH_2)_n + nH_2O$

The fraction of each hydrocarbon is given by the Anderson Schulz Flory distribution shown in the following equation.

$m_n = (1-\alpha)\alpha^{n-1}$

where, m_n is the fraction of the hydrocarbon product with chain length n and α is the probability of chain propagation given by:

$$\alpha = \frac{R_p}{R_p + R_t}$$

where, R_p and R_t are rates of propagation and termination. Typical reported ranges of α on Ru, Co, and Fe of 0.85–0.95, 0.70–0.80, and 0.50–0.70, respectively.

Syngas Consumption

Considering the overall reactions such that x is the average carbon number and y is the average hydrogen number in the hydrocarbon produced.

$CO + (1+y/2x)\,H_2 \rightarrow C_xH_y + H_2O$ (FT)

The water produced during the reaction may react with the carbon monoxide via the water gas shift reaction.

$CO + H_2O \rightarrow CO_2 + H_2$ (WGS)

The rate of syngas consumption $(-R_{syngas})$ is the sum of the rate of consumption of CO and rate of consumption of H_2. The mean rate of FT synthesis (R_{FT}) is given by the following relationship.

$$-\boldsymbol{R}_{\boldsymbol{syngas}} = \left(2 + \frac{\boldsymbol{y}}{2\boldsymbol{x}}\right)\boldsymbol{R}_{\boldsymbol{FT}}$$

The following table tabulates some of the rate equations for the FT synthesis cited in literature:

Table 1 Rate forms of overall FT synthesis

1	kP_{H_2}	low syngas conversion, high WGS
2	$kP_{H_2}P_{CO}$	high syngas conversion
3	$kP_{H_2}{}^{a}P_{CO}{}^{b}$	empirical form of Eq. 2
4	$\frac{kP_{hyd}P_{CO}}{P_{CO}+aP_{H_2O}}$	water inhibition
5	$\frac{kP_{hyd}{}^{2}P_{CO}}{P_{CO}P_{hyd}+aP_{H_2O}}$	water inhibition
6	$\frac{kP_{hyd}{}^{2}P_{CO}}{1+aP_{CO}P_{hyd}{}^{2}}$	
7	$\frac{kP_{hyd}P_{CO}}{P_{CO}+aP_{CO_2}}$	carbon dioxide inhibition
8	$\frac{kP_{hyd}P_{CO}}{P_{CO}+aP_{H_2O}+bP_{CO_2}}$	both water and carbon dioxide inhibition
9	$\frac{kP_{hyd}P_{CO}}{(1+P_{CO})^{2}}$	

For the hydrocarbon formation, the following rate for CO consumption has been suggested in literature.

$$-R_{CO}=\frac{kP_{hyd}{}^{a}P_{CO}{}^{b}}{(1+\sum K_j P_{hyd}^{c_j}P_{CO}^{d_j})^2}$$

where k is the kinetic rate constant following the Arhennius' law, a and b are the reaction orders, K_j is the adsorption coefficient of the j^{th} adsorption term, c_j and d_j are the dependency of the surface coverage on the reaction pressure of the j^{th} adsorption term.

Water Gas Shift Reaction

The water gas shift reaction in conjunction with the FT reaction provides us with the kinetic rate data on water generation, CO_2 generation, CO depletion and the hydrogen mass balance. Several forms of the water gas shift reaction are available. The most common relationship among those reported is:

$$R_{WGS}=R_{CO_2}=k_w\left(P_{CO}P_{H_2O}-\frac{P_{CO_2}P_{H_2}}{K_{WGS}}\right)$$

where k_w is the reaction rate constant of the forward shift and K_{wgs} is the equilibrium constant given by:

$$\log(K_{wgs}) = \log\frac{P_{H_2}P_{CO_2}}{P_{CO}P_{H_2O}} = \left(\frac{2073}{T} - 2.029\right).$$

Hydrocarbon Generation

The rate of generation of a hydrocarbon with a carbon number of *n* can be described by a power law form as shown below.

$$R_n = k_n P_{H_2}{}^a P_{CO}{}^b$$

If one were to assume the ASF distribution, the rate can be rewritten for *n* = 2 to7, by the following.

$$R_n = R_{CH_4}\alpha^{n-1}$$

where,

$$R_{CH_4} = k_1 P_{H_2}{}^3 P_{CO}.$$

Applying polymerization principles, some researchers have reported the following terms for initiation and termination.

$$R_{ini} = k_H \theta_H \theta_{CH_2}$$

and

$$R_{ter} = k_{parhyd}\theta_H \sum_1^m \theta_{R_{ini}} + k_{parmeth}\theta_{CH_3}\sum_1^m \theta_{R_{ini}}$$

Further analysis by Zimmermann yielded the following.

Initiation

$$R_i = k_p \theta_H{}^2 \theta_{CO}$$

Propagation

$$R_{p,i} = k_p \theta_i \theta_{CO} \theta_H \qquad \text{i} = 1 \rightarrow \text{N}$$

Termination

Methane

$$R_{para,1} = (k_{t,para}\theta_H + k_{t,olef})\theta_1$$

Paraffins

$$R_{para,i} = k_{t,para}\theta_H\theta_i \qquad \text{i = 2} \rightarrow \text{N}$$

Olefins

$$R_{olef,i} = k_{t,olef}\left(\theta_i - \frac{P_{C_iH_{2i}}\theta_H}{k_e}\right) \qquad \text{i = 2} \rightarrow \text{N}$$

Secondary Hydrogenation Reaction

$$R_{s,i} = \frac{k_s P_{H_2} P_{C_iH_{2i}}}{1 + \left(K_{H_2} P_{H_2}\right)^{1/2}\left(1 + \sum_j^N K_e P_{C_jH_{2j}}\right)^2}$$

Water Gas Shift

$$R_{WGS} = R_{CO_2} = k_w\left(P_{CO}P_{H_2O} - \frac{P_{CO_2}P_{H_2}}{K_{WGS}}\right)$$

The above forms were used for the species generation/consumption by reaction component in the mass transfer model.

Task 2. Data Collection

Data on fluidized bed FT synthesis were collected throughout the duration of this project. Some of the data are reported herein. Data from work done by Fujimoto and his researchers (Fujimoto et al, 2004) were analyzed. The plot of selectivites towards the formation of a hydrocarbon vs. carbon chain length is presented in Figure 1. The highest selectivities are observed to be in the range of carbon numbers between 4 -7. The reaction conditions are provided in Table 2. The observed CO conversion was 47.3 %. A summary of the process condition and product data from the research conducted by Hall in 1949 is provided in Table 3. Experiments were conducted at 20 atm and 300 ^{o}C. The H_2:CO ratio used was greater than the stoichiometrically required. Near complete CO conversion was observed with no CO_2 produced. Demeter conducted several experiments in 1959. A substantial amount of data was recently found on www.fisher-tropsch.org that contains data on the fluidized bed tests conducted by Texaco-Chevron.

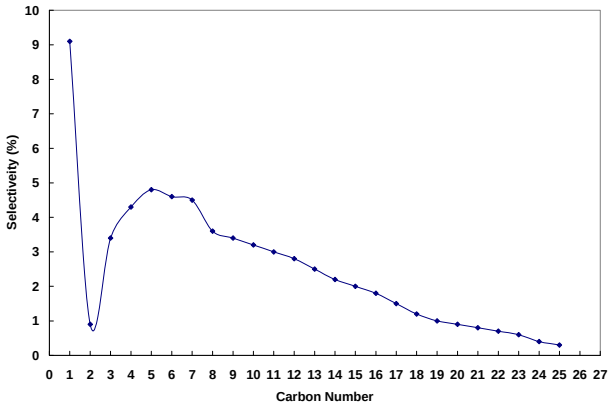

Figure 1

Table 2 Fluidized bed FT synthesis data (1).

Fluidized Bed Reactor Conditions:	
T (ºC)	240
P_{TOTAL} (MPa)	4.5
P_{HEXANE} (MPa)	3.5
P_{SYNGAS} (MPa)	1
W/F (g cat.h/mol)	5
Conversion	
CO (%)	47.3

Table 3 Fluidized bed FT synthesis data (2)

Fluidized Bed - High Space Velocities:		
T (ºC)	300	300
$P_{REACTOR}$ (atm gauge)	20	20
Syngas Ratio (H_2:CO)	2.31	2.34
Conversion		
CO (%)	99.1	99.5
Selectivities		
Carbon Number		
CO_2	0	0
CH_4	19.9	20.9
C_2-C_{25}	80.1	79.1
Yield (Selectivities)		
Carbon Number	Yield (gm/m^3)	
CH_4	40.2	42.4
C_2-C_4	104.4	106.7
Liquid Hydrocarbons	33.3	31.7
Higher Hydrocarbons	137.7	138.4

Table 4 Fluidized bed FT synthesis data (3).

Fluidized Bed Reactor Conditions

Catalyst Age (hr)	0	30	54	78	168	240	336	411	576	649	742	814
Pressure (psi)	100	150	200	300	300	300	300	300	300	300	300	300
T (ºC)	238	239	239	238	240	250	251	252	252	252	252	253
Recycle to Fresh Gas Ratio	3:1	3:1	3:1	3:1	6:1	6:1	9:1	12:1	10:1	8:1	12:1	9:1
Syngas Ratio (H_2:CO)	1:1	1:1	1:1	1:1	1:1	1:1	1:1	1:1	1:1	1:1	0.97:1	1:1

Conversion

H_2 (%)	27.5	21.4	20.2	27.5	41.2	54.7	73.6	82	82.1	80.2	86.4	67.5
CO (%)	21.4	15.2	15.1	21.2	28.1	42.1	62.7	74.4	78	76.2	83.5	54
H_2+CO (%)	24.4	18.3	17.7	24.3	34.6	48.4	68	78.3	80	77.7	84.9	60.8

Yield (Selectivities)

Carbon Number	Yield (gm/m^3)											
CH_4	43.65	44.39	52.91	34.87	47.25	47.52	50.82	51.53	48.73	52.03	44.64	45.2
C_2	27.28	25.34	26.31	12.94	22.84	23.17	23.44	23.83	24.41	21.9	18.56	17.1
C_3	39.29	36.94	38.17	37.74	36.93	36.01	29.53	27.18	22.94	22.81	20.91	34.8
C_4	36.01	46.36	15.4	25.16	27.17	16.92	21.33	20.79	24.19	16.29	14.88	16.1
C_5	10.91	14.8	0	0	6.64	0	4.8	7.36	17.52	3.6	4.17	8.5

Task 3. Conceptual Design of Model Reactor

Let us consider a cylindrical reactor system as shown in Figure 2.

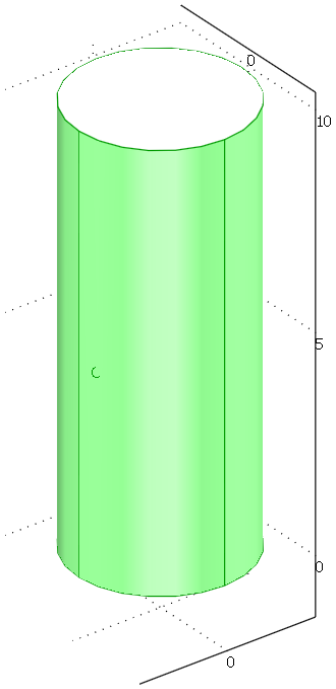

Figure 2 FT fluid bed reactor model (b)

The reactor parameters to be considered are provided in Table 5 and the inlet gas composition is given in Table 6.

Table 5 Simulation Parameters

Reactor Dimensions	(a)	(b)
Length	2.5 m	10 m
Diameter	0.05 m	2 m
Inlet Conditions		
Temperature	573 K	
Pressure	10×10^{5} Pa	
Volumetric Gas Flowrate	4×10^{-3} m^3/min	
Catalyst mass	200×10^{-3}g	
Solids Properties		
FT catalyst mean particle size	100×10^{-6} m	
FT catalyst density	1600 kg/m^3	
*Cracking catalyst mean particle size	75×10^{-6}m	
*Cracking catalyst density	2200 kg/m^3	

* Not used in the model runs

Table 6 Feed Composition

Inlet Gas Composition:	
CO	33 %
H_2	67 %
Inert	0 %
CO_2	0 %
H_2O	0 %
C_xH_y	0 %

Task 4. Dynamic Population Balance Model Development

Based on the above information, a model has been developed to predict the performance of a fluidized bed reactor with respect to FT synthesis and cracking.

Mass Balance

In the research problem, there are 3 phases (p), namely gas phase (g), FT catalyst phase (FT) and the cracking catalyst phase (crack). In addition to the 3 phases, the species that have to be considered for the process are carbon monoxide (CO), hydrogen (H_2), carbon dioxide (CO_2), steam (H_2O), inerts (I), methane (CH_4) and (N-1) hydrocarbons from C_2 – C_N. Several other species of hydrocarbons can be included in the general model. Thus, the number of species (*k*) is equal to 5 + N.

Taking a slice of the cylinder shown above with coordinates of (r, θ, z), ((r, θ +Δθ, z), (r + Δ r, θ, z), (r, θ, z + Δ z), (r + Δ r, θ + Δθ, z), (r + Δ r, θ, z + Δ z), (r, θ + Δθ, z + Δ z), and (r + Δ r, θ + Δθ, z + Δ z), where r = 0 at the axis of the cylinder and z = 0 at the bottom of the cylinder. The slice is shown below in Figure 3.

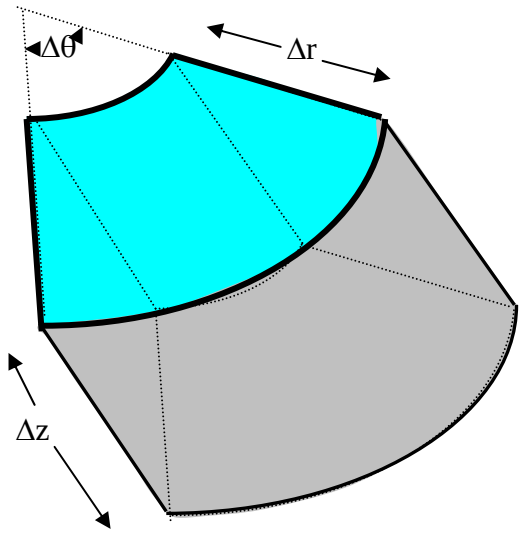

Figure 3 Elemental volume in the reactor.

In general mass balance can be written as

Mass Flux in + Generation/Consumption = Mass Flux Out + Accumulation

There are 5 components of mass transfer by component *k*: (a) component *k* enters and leaves the unit elemental volume by gas convection, (b) component *k* enters and leaves the unit elemental volume by FT catalyst convection, (c) component *k* enters of leaves the unit elemental volume by cracking catalyst convection, (d) component *k* enters or leaves the unit elemental volume by diffusion, (e) generation/disappearance of component *k* by reaction on the FT catalyst (subscript FT), and (f) generation/disappearance of component *k* by reaction on the cracking catalyst (subscript crack). The following generalized mass balance can be written for phase *p* based on the above discussion.

$$\Delta\, Diffusive_{gas} + \Delta\, Convective_{gas} + \Delta\, Convective_{FT} + \Delta\, Convective_{crack} + Chemical\ Reaction_{FT} + Chemical\ Reaction_{crack} = [Accumulation]_{(gas+FT+crack)}$$

Consider the unit elementary volume in cylindrical coordinates with dimensions of Δr, $\Delta\theta$ and Δz. The terms for component *k* in phase *p* are shown below.

Diffusive transport

$$\varepsilon_g \left[\begin{array}{l} r\Delta\theta\Delta z\left\{\left(N_{k,r}\right)_{r,\theta,z} - \left(N_{k,r}\right)_{r+\Delta r,\theta,z}\right\} + \Delta r\Delta z\left\{\left(N_{k,\theta}\right)_{r,\theta,z} - \left(N_{k,\theta}\right)_{r,\theta+\Delta\theta,z}\right\} \\ + r\Delta\theta\Delta r\left\{\left(N_{k,z}\right)_{r,\theta,z} - \left(N_{k,z}\right)_{r,\theta,z+\Delta z}\right\} \end{array} \right]$$

where $N_{k,}$ is the molar flux of species *k* following Fick's diffusion.

Gas Convection

$$\varepsilon_g \left[\begin{array}{l} \boldsymbol{r}\Delta\theta\Delta\boldsymbol{z}\left\{\left(\boldsymbol{U}_{\boldsymbol{gas,r}} \bullet \boldsymbol{C}_{\boldsymbol{k}}\right)_{\boldsymbol{r},\theta,\boldsymbol{z}} - \left(\boldsymbol{U}_{\boldsymbol{gas,r}} \bullet \boldsymbol{C}_{\boldsymbol{k}}\right)_{\boldsymbol{r}+\Delta\boldsymbol{r},\theta,\boldsymbol{z}}\right\} + \Delta\boldsymbol{r}\Delta\boldsymbol{z}\left\{\left(\boldsymbol{U}_{\boldsymbol{gas},\theta} \bullet \boldsymbol{C}_{\boldsymbol{k}}\right)_{\boldsymbol{r},\theta,\boldsymbol{z}} - \left(\boldsymbol{U}_{\boldsymbol{gas},\theta} \bullet \boldsymbol{C}_{\boldsymbol{k}}\right)_{\boldsymbol{r},\theta+\Delta\theta,\boldsymbol{z}}\right\} \\ + \boldsymbol{r}\Delta\theta\Delta\boldsymbol{r}\left\{\left(\boldsymbol{U}_{\boldsymbol{gas,z}} \bullet \boldsymbol{C}_{\boldsymbol{k,p}}\right)_{\boldsymbol{r},\theta,\boldsymbol{z}} - \left(\boldsymbol{U}_{\boldsymbol{gas,z}} \bullet \boldsymbol{C}_{\boldsymbol{k}}\right)_{\boldsymbol{r},\theta,\boldsymbol{z}+\Delta\boldsymbol{z}}\right\} \end{array} \right]$$

where ε_g is the void fraction, U_{gas} is the convective velocity of the gas along the direction given in the subscript and C_k is the concentration of component *k* in the gas phase.

Convection of FT catalyst

If the void fraction is ε_g, then $(1-\varepsilon_g)$ is the fraction of solids in that unit volume. Let us assume that λ is the fraction of the solids that consists of the cracking catalyst in the elemental volume, then the transport of species *k* on the catalyst surface by convective transport of the FT catalyst is given by:

$$(1-\varepsilon_g)(1-\lambda)\begin{bmatrix} r\Delta\theta\Delta z\left\{\left(U_{FT,r}\bullet S_{FT}\bullet\Theta_{k,FT}\right)_{r,\theta,z}-\left(U_{FT,r}\bullet S_{FT}\bullet\Theta_{k,FT}\right)_{r+\Delta r,\theta,z}\right\} \\ +\Delta r\Delta z\left\{\left(U_{FT,\theta}\bullet S_{FT}\bullet\Theta_{k,FT}\right)_{r,\theta,z}-\left(U_{FT,\theta}\bullet S_{FT}\bullet\Theta_{k,FT}\right)_{r,\theta+\Delta\theta,z}\right\} \\ +A_z\left\{\left(U_{FT,z}\bullet S_{FT}\bullet\Theta_{k,FT}\right)_{r,\theta,z}-\left(U_{FT,z}\bullet S_{FT}\bullet\Theta_{k,FT}\right)_{r,\theta,z+\Delta z}\right\} \end{bmatrix}$$

$$\Theta_{k,FT}=f_1(C_k)$$

where S_{FT} is the occupied FT catalyst surface area per unit volume, $\Theta_{k,FT}$ is the concentration of species k on FT catalyst surface per unit FT catalyst surface area, and λ is the fraction of solids in the unit elementary volume comprising the cracking catalyst. The total surface of the FT catalyst occupied is given by the extended Langmuir model for adsorption of species.

$$\boldsymbol{S_{FT}}=\frac{\beta_{\boldsymbol{FT}}\boldsymbol{*}\sum_{\boldsymbol{k}=1}^{\boldsymbol{k}=\boldsymbol{N}+5}\boldsymbol{K_{k,FT}}\cdot\boldsymbol{C_k}}{1+\sum_{\boldsymbol{k}=1}^{\boldsymbol{k}=\boldsymbol{N}+5}\boldsymbol{K_{k,FT}}\cdot\boldsymbol{C_k}},$$

where β_{FT} is the maximum surface area per unit volume available at the start of the process, $K_{k,FT}$ are the adsorption coefficients for each species k and C_k is the concentration of the species in the gas phase.

Convection of cracking catalyst

Similar to the case of the FT catalyst, transport of species k due to the convective transport of the cracking catalyst is given by:

$$(1-\varepsilon_g)(\lambda)\begin{bmatrix} r\Delta\theta\Delta z\left\{\left(U_{crack,r}\bullet S_{crack}\bullet\Theta_{k,crack}\right)_{r,\theta,z}-\left(U_{crack,r}\bullet S_{cracp}\bullet\Theta_{k,crack}\right)_{r+\Delta r,\theta,z}\right\} \\ +\Delta r\Delta z\left\{\left(U_{crack,\theta}\bullet S_{crack}\bullet\Theta_{k,crack}\right)_{r,\theta,z}-\left(U_{crack,\theta}\bullet S_{crack}\bullet\Theta_{k,crack}\right)_{r,\theta+\Delta\theta,z}\right\} \\ +r\Delta\theta\Delta r\left\{\left(U_{crack,z}\bullet S_{crack}\bullet\Theta_{k,crack}\right)_{r,\theta,z}-\left(U_{crack,z}\bullet S_{crack}\bullet\Theta_{k,crack}\right)_{r,\theta,z+\Delta z}\right\} \end{bmatrix}$$

$$\Theta_{k,crack}=f_2(C_k)$$

where S_{crack} is the occupied cracking catalyst surface area per unit volume, and $\Theta_{k,crack,}$ is the concentration of species k on the cracking catalyst surface per unit cracking catalyst surface area.

Similar to the case of the FT catalyst, the total surface of the FT catalyst occupied is given by the extended Langmuir model for adsorption of species.

$$S_{crack} = \frac{\beta_{crack} * \sum_{k=1}^{k=N+5} K_{k,crack} \cdot C_k}{1 + \sum_{k=1}^{k=N+5} K_{k,crack} \cdot C_k},$$

where β_{crack} is the maximum surface area per unit volume available at the start of the process, $K_{k,crack}$ are the adsorption coefficients for each species k and C_k is the concentration of the species in the gas phase.

Chemical reaction on FT catalyst

In addition to the transport of species by physical means into and out of the elemental volume, species are generated or depleted from elemental volume by chemical reaction. In the proposed process, these reactions take place on the FT and the cracking catalyst. The reactions on the FT catalyst are given below:

$$\Delta V(1-\varepsilon_g)(1-\lambda)\rho_{FT}\left[\sum_{l=1}^{N_{react,FT}} n_{k,l} \bullet \eta_{l,FT,p} \bullet R_{k,l,FT}\right]$$

where ΔV is the volume of the elementary volume, $n_{k,l}$ is the stoichiometric coefficient of species k for reaction l, $R_{k,l}$ is the rate of reaction l with respect to species k, $\eta_{l,p}$ is the effectiveness factor for reaction l for species k, $N_{react,\ FT}$ is the total number of FT reactions and ρ_{FT} is density of the FT catalyst. In cylindrical coordinates the above can be rewritten as:

$$r\Delta r\Delta\theta\Delta z(1-\varepsilon_g)(1-\lambda)\rho_{FT}\left[\sum_{l=1}^{N_{react,FT}} n_{k,l} \bullet \eta_{l,FT,p} \bullet R_{k,l,FT}\right].$$

Chemical Reaction on Cracking Catalyst

Similarly, for calculating mass generated or depleted of species k by reaction on the cracking catalyst, the mathematical expression is:

$$r\Delta r\Delta\theta\Delta z(1-\varepsilon_g)(\lambda)\rho_{crack}\left[\sum_{l=1}^{N_{react,crack}} n_{k,l} \bullet \eta_{l,crack,p} \bullet R_{k,l,crack}\right]$$

where the subscript *crack* is for the cracking catalyst.

Accumulation

Finally, the last component of the balance is given by the accumulation term as shown below:

$$r\Delta r\Delta\theta\Delta z\left[\varepsilon_g \frac{\partial C_k}{\partial t} + (1-\varepsilon_g)(1-\lambda\ )S_{FT}\frac{\partial \Theta_{k,FT}}{\partial t} + (1-\varepsilon_g)(1-\lambda)S_{crack}\frac{\partial \Theta_{k,crack}}{\partial t}\right].$$

Summing the components of mass balance and dividing each component by rΔrΔzΔθ, the overall mass balance (in molar terms) obtained for species k is given by:

$$\left[\varepsilon_g \frac{\partial \boldsymbol{C}_k}{\partial \boldsymbol{t}} + (1-\varepsilon_g)(1-\lambda)\boldsymbol{S}_{FT}\frac{\partial \boldsymbol{f}_1(\boldsymbol{C}_k)}{\partial \boldsymbol{t}} + (1-\varepsilon_p)(\lambda_p)\boldsymbol{S}_{crack}\frac{\partial \boldsymbol{f}_2(\boldsymbol{C}_k)}{\partial \boldsymbol{t}}\right] =$$

$$\varepsilon_g\left\{\left[\frac{1}{\boldsymbol{r}}\frac{\partial(\boldsymbol{r}\bullet \boldsymbol{N}_{k,r})}{\partial \boldsymbol{r}} + \frac{1}{\boldsymbol{r}}\frac{\partial \boldsymbol{N}_{k,\theta}}{\partial \theta} + \frac{\partial \boldsymbol{N}_{k,p,x}}{\partial \boldsymbol{z}}\right] + \left[\frac{1}{\boldsymbol{r}}\frac{\partial(\boldsymbol{r}\bullet \boldsymbol{U}_r \bullet \boldsymbol{C}_k)}{\partial \boldsymbol{r}} + \frac{1}{\boldsymbol{r}}\frac{\partial(\boldsymbol{U}_\theta \bullet \boldsymbol{C}_k)}{\partial \theta} + \frac{\partial(\boldsymbol{U}_z \bullet \boldsymbol{C}_k)}{\partial \boldsymbol{z}}\right]\right\}$$

$$+(1-\varepsilon_g)(1-\lambda)\left[\frac{1}{\boldsymbol{r}}\frac{\partial(\boldsymbol{r}\bullet \boldsymbol{S}_{FT}\bullet \boldsymbol{U}_{FT,r}\bullet \boldsymbol{f}_1(\boldsymbol{C}_k))}{\partial \boldsymbol{r}} + \frac{1}{\boldsymbol{r}}\frac{\partial(\boldsymbol{S}_{FT}\bullet \boldsymbol{U}_{FT,\theta}\bullet \boldsymbol{f}_1(\boldsymbol{C}_k))}{\partial \theta} + \frac{\partial(\boldsymbol{S}_{FT}\bullet \boldsymbol{U}_{FT,z}\bullet \boldsymbol{f}_1(\boldsymbol{C}_k))}{\partial \boldsymbol{z}}\right]$$

$$+(1-\varepsilon_g)(\lambda)\left[\frac{1}{\boldsymbol{r}}\frac{\partial(\boldsymbol{r}\bullet \boldsymbol{S}_{crack}\bullet \boldsymbol{U}_{crack,r}\bullet \boldsymbol{f}_2(\boldsymbol{C}_k))}{\partial \boldsymbol{x}} + \frac{1}{\boldsymbol{r}}\frac{\partial(\boldsymbol{S}_{crack}\bullet \boldsymbol{U}_{crack,\theta}\bullet \boldsymbol{f}_2(\boldsymbol{C}_k))}{\partial \theta} + \frac{\partial(\boldsymbol{S}_{crack}\bullet \boldsymbol{U}_{crack,z}\bullet \boldsymbol{f}_2(\boldsymbol{C}_k))}{\partial \boldsymbol{z}}\right]$$

$$+\left[(1-\varepsilon\ )(1-\lambda)\rho_{FT}\sum_{l=1}^{N_{reac,FTt}}\boldsymbol{n}_{k,l}\bullet \eta_{l,FT}\bullet \boldsymbol{R}_{k,l,FT}\right] + \left[(1-\varepsilon_g)(\lambda)\rho_{crack}\sum_{l=1}^{N_{reac,crackt}}\boldsymbol{n}_{k,l}\bullet \eta_{l,crack}\bullet \boldsymbol{R}_{k,l,crack}\right].$$

Rewriting the diffusive fluxes $\partial rN_r/\partial r,\quad \partial N_\theta/\partial\theta, \partial N_z/\partial z,$

$$\frac{1}{r}\frac{\partial rN_r}{\partial r} = \frac{-D}{r}\frac{\partial}{\partial r}\left(r\frac{\partial C}{\partial r}\right)$$

$$\frac{\partial N_\theta}{\partial r} = -D\frac{\partial}{\partial \theta}\left(\frac{\partial C}{\partial \theta}\right)$$

$$\frac{\partial N_z}{\partial r} = -D\frac{\partial}{\partial z}\left(\frac{\partial C}{\partial z}\right)$$

Where, D is the diffusivity.

The surface coverage of species *k* on the FT catalyst and the cracking catalyst surface are given by:

$$\Theta_{k,FT} = \boldsymbol{f}_1(\boldsymbol{C}_k) = \frac{\boldsymbol{K}_{k,FT}\cdot \boldsymbol{C}_k}{1+\sum_{j=1}^{j=N+5}\boldsymbol{K}_{j,FT}\cdot \boldsymbol{C}_j}$$

and

$$\Theta_{k,crack} = \boldsymbol{f}_1(\boldsymbol{C}_k) = \frac{\boldsymbol{K}_{k,crack}\cdot \boldsymbol{C}_k}{1+\sum_{j=1}^{j=N+5}\boldsymbol{K}_{j,crack}\cdot \boldsymbol{C}_j}.$$

Replacing these functions in the overall equation we obtain:

$$\left[\varepsilon_g \frac{\partial \boldsymbol{C}_k}{\partial t} + (1-\varepsilon_g)(1-\lambda)\frac{\beta_{FT} \bullet \sum_1^{N+5} \boldsymbol{K}_{j,FT}\boldsymbol{C}_j}{1+\sum_1^{N+5} \boldsymbol{K}_{j,FT}\boldsymbol{C}_j}\frac{\partial \boldsymbol{f}_1(\boldsymbol{C}_k)}{\partial t} + (1-\varepsilon_p)(\lambda_p)\frac{\beta_{crack} \bullet \sum_1^{N+5} \boldsymbol{K}_{j,crack}\boldsymbol{C}_j}{1+\sum_1^{N+5} \boldsymbol{K}_{j,crack}\boldsymbol{C}_j}\frac{\partial \boldsymbol{f}_2(\boldsymbol{C}_k)}{\partial t}\right] =$$

$$\varepsilon_g\left\{\left[\frac{1}{\boldsymbol{r}}\frac{\partial}{\partial \boldsymbol{r}}\left(\boldsymbol{r}\frac{\partial \boldsymbol{C}_k}{\partial \boldsymbol{r}}\right)+\frac{1}{\boldsymbol{r}}\frac{\partial}{\partial \theta}\left(\frac{\partial \boldsymbol{C}_k}{\partial \theta}\right)+\frac{\partial}{\partial \boldsymbol{z}}\left(\frac{\partial \boldsymbol{C}_k}{\partial \boldsymbol{z}}\right)\right]+\left[\frac{1}{\boldsymbol{r}}\frac{\partial\left(\boldsymbol{r}\bullet \boldsymbol{U}_r \bullet \boldsymbol{C}_k\right)}{\partial \boldsymbol{r}}+\frac{1}{\boldsymbol{r}}\frac{\partial\left(\boldsymbol{U}_\theta \bullet \boldsymbol{C}_k\right)}{\partial \theta}+\frac{\partial\left(\boldsymbol{U}_z \bullet \boldsymbol{C}_k\right)}{\partial \boldsymbol{z}}\right]\right\}$$

$$+(1-\varepsilon_g)(1-\lambda)\left[\begin{array}{l}\dfrac{1}{\boldsymbol{r}}\dfrac{\partial\left(\boldsymbol{r}\bullet\dfrac{\beta_{FT}\bullet\sum_1^{N+5}\boldsymbol{K}_{j,FT}\boldsymbol{C}_j}{1+\sum_1^{N+5}\boldsymbol{K}_{j,FT}\boldsymbol{C}_j}\bullet\boldsymbol{U}_{FT,r}\bullet\dfrac{\boldsymbol{K}_{k,FT}\boldsymbol{C}_k}{1+\sum_1^{N+5}\boldsymbol{K}_{j,FT}\boldsymbol{C}_j}\right)}{\partial \boldsymbol{r}} \\ +\dfrac{1}{\boldsymbol{r}}\dfrac{\partial\left(\dfrac{\beta_{FT}\bullet\sum_1^{N+5}\boldsymbol{K}_{j,FT}\boldsymbol{C}_j}{1+\sum_1^{N+5}\boldsymbol{K}_j\boldsymbol{C}_j}\bullet\boldsymbol{U}_{FT,\theta}\bullet\dfrac{\boldsymbol{K}_{k,FT}\boldsymbol{C}_k}{1+\sum_1^{N+5}\boldsymbol{K}_{j,FT}\boldsymbol{C}_j}\right)}{\partial \theta} \\ +\dfrac{\partial\left(\dfrac{\beta_{FT}\bullet\sum_1^{N+5}\boldsymbol{K}_{j,FT}\boldsymbol{C}_j}{1+\sum_1^{N+5}\boldsymbol{K}_{j,FT}\boldsymbol{C}_j}\bullet\boldsymbol{U}_{FT,z}\bullet\dfrac{\boldsymbol{K}_{k,FT}\boldsymbol{C}_k}{1+\sum_1^{N+5}\boldsymbol{K}_{j,FT}\boldsymbol{C}_j}\right)}{\partial \boldsymbol{z}}\end{array}\right]$$

$$+(1-\varepsilon_g)(\lambda)\left[\begin{array}{l}\dfrac{1}{\boldsymbol{r}}\dfrac{\partial\left(\boldsymbol{r}\bullet\dfrac{\beta_{crack}\bullet\sum_1^{N+5}\boldsymbol{K}_{j,crack}\boldsymbol{C}_j}{1+\sum_1^{m+k}\boldsymbol{K}_{j,crack}\boldsymbol{C}_j}\bullet\boldsymbol{U}_{crack,r}\bullet\dfrac{\boldsymbol{K}_{k,crack}\boldsymbol{C}_j}{1+\sum_1^{N+5}\boldsymbol{K}_{j,crack}\boldsymbol{C}_j}\right)}{\partial \boldsymbol{x}} \\ +\dfrac{1}{\boldsymbol{r}}\dfrac{\partial\left(\dfrac{\beta_{crack}\bullet\sum_1^{N+5}\boldsymbol{K}_{j,crack}\boldsymbol{C}_j}{1+\sum_1^{m+k}\boldsymbol{K}_{j,crack}\boldsymbol{C}_j}\bullet\boldsymbol{U}_{crack,\theta}\bullet\dfrac{\boldsymbol{K}_{k,crack}\boldsymbol{C}_j}{1+\sum_1^{m+k}\boldsymbol{K}_{j,crack}\boldsymbol{C}_j}\right)}{\partial \theta} \\ +\dfrac{\partial\left(\dfrac{\beta_{crack}\bullet\sum_1^{N+5}\boldsymbol{K}_{j,crack}\boldsymbol{C}_j}{1+\sum_1^{N+5}\boldsymbol{K}_{j,crack}\boldsymbol{C}_j}\bullet\boldsymbol{U}_{crack,z}\bullet\dfrac{\boldsymbol{K}_{k,crack}\boldsymbol{C}_j}{1+\sum_1^{N+5}\boldsymbol{K}_{j,crack}\boldsymbol{C}_j}\right)}{\partial \boldsymbol{z}}\end{array}\right]$$

$$+\left[(1-\varepsilon\ )(1-\lambda)\rho_{FT}\sum_{l=1}^{N_{reac,FTt}}\boldsymbol{n}_{k,l}\bullet\eta_{l,FT}\bullet\boldsymbol{R}_{k,l,FT}\right]+\left[(1-\varepsilon_g)(\lambda)\rho_{crack}\sum_{l=1}^{N_{reac,crackt}}\boldsymbol{n}_{k,l}\bullet\eta_{l,crack}\bullet\boldsymbol{R}_{k,l,crack}\right]$$

Since the differential volume has no interaction with the surroundings, the boundary conditions then provide the conditions of the interchange of the species with the surrounding. A simplistic set of boundary and initial conditions are provided in Table 7.

Table 7 Initial and Boundary Conditions

r=0	$\frac{\partial \boldsymbol{C_k}}{\partial \boldsymbol{r}} = 0$
r=D/2	$\frac{\partial \boldsymbol{C_k}}{\partial \boldsymbol{r}} = 0$
z=0	$-\boldsymbol{D_{k,z}} \frac{\partial \boldsymbol{C_k}}{\partial \boldsymbol{z}} = \boldsymbol{U_g}(\boldsymbol{C_{k,0-}} - \boldsymbol{C_{k,0+}})$
z=L	$\frac{\partial \boldsymbol{C_k}}{\partial \boldsymbol{z}} = 0$
T=0	$C_k = C_{k,o}$

The model developed was used in conjunction with axial and lateral mixing models based on counter current back mixing models already developed for several applications. The extension of the model is not shown. However, the basic idea is to divide the elemental volume longitudinally into two compartments, one in which the solids are moving upwards and in the other solids are moving downwards. Mass transfer between these two compartments was considered.

FORCE BALANCE

Force balance in the *z* direction yields

$$-\frac{dP_p}{dz} = \varepsilon_p \rho_{gas} g + (1-\varepsilon_p)(1-\lambda_p)\rho_{FT} \bullet g + (1-\varepsilon_p)(\lambda_p)\rho_{crack} g$$

Energy Balance

In general, the energy balance can be written as

Heat Flux In + Generation/Consumption = Heat Flux Out + Accumulation

Similar to the steps taken to derive the mass balance equation, the energy balance was derived. The overall balance considering $\bar{U}$, the internal energy, ΔH, the heat of the reaction, N_{react}, the total number of reactions, N_{comp} $(=N+5)$, the total number of species, and q is the heat flux by diffusion is given by

$$
\begin{bmatrix}
\varepsilon_g \frac{\partial}{\partial t} \sum_{j=1}^{m} C_k \bullet \ddot{U}_k + (1-\varepsilon_g)(1-\lambda\ ) \frac{\partial}{\partial t}\left(S_{FT} \sum_{j=1}^{m} f_1(C_j) \bullet \ddot{U}_{j,FT} \right) \\
+ (1-\varepsilon_g)(\lambda\ ) \frac{\partial}{\partial t}\left(S_{crack} \sum_{j=1}^{m} f_2(C_j) \bullet \ddot{U}_{j,crack} \right) \\
+ (1-\varepsilon_g)(1-\lambda\ ) \frac{\partial\left(\rho_{FT} \bullet \ddot{U}_{FT}\right)}{\partial t} + (1-\varepsilon_g)(\lambda\ ) \frac{\partial\left(\rho_{crack} \bullet \ddot{U}_{crack}\right)}{\partial t}
\end{bmatrix} =
$$

$$
\varepsilon_g \left\{ \left[\frac{1}{r}\frac{\partial rq}{\partial r} r + \frac{1}{r}\frac{\partial q}{\partial \theta} + \frac{\partial q}{\partial z} \right] + \begin{bmatrix} \frac{1}{r}\frac{\partial}{\partial r} r U_r \sum_{j=1}^{m} C_j \bullet \ddot{U}_j + \frac{1}{r}\frac{\partial}{\partial \theta} U_\theta \sum_{j=1}^{m} C_j \bullet \ddot{U}_j \\ + \frac{\partial}{\partial z} U_z \sum_{j=1}^{m} C_j \bullet \ddot{U}_j \end{bmatrix} \right\}
$$

$$
+ (1-\varepsilon_g)(1-\lambda\ ) \begin{bmatrix} \frac{1}{r}\frac{\partial}{\partial r} r U_{FT,r} \bullet S_{FT} \sum_{j=1}^{Ncomp} f_1(C_j) \bullet \ddot{U}_j \\ + \frac{\partial}{\partial \theta} U_{FT,\theta} \bullet S_{FT} \sum_{j=1}^{Ncomp} f_1(C_j) \bullet \ddot{U}_j \\ + \frac{\partial f}{\partial z} U_{FT,z} \bullet S_{FT,} \sum_{j=1}^{Ncomp} f_1(C_j) \bullet \ddot{U}_j \end{bmatrix}
$$

$$
+ (1-\varepsilon_g)(1-\lambda\ ) \begin{bmatrix} \frac{1}{r}\frac{\partial\left(r \bullet U_{FT,r} \bullet \rho_{FT} \bullet \ddot{U}_{FT}\right)}{\partial r} + \frac{1}{r}\frac{\partial\left(U_{FT,\theta} \bullet \rho_{FT} \bullet \ddot{U}_{FT}\right)}{\partial \theta} \\ + \frac{\partial\left(U_{FT,z} \bullet \rho_{FT} \bullet \ddot{U}_{FT}\right)}{\partial z} \end{bmatrix}
$$

$$
+ (1-\varepsilon_g)(\lambda\ ) \begin{bmatrix} \frac{1}{r}\frac{\partial}{\partial r} r \bullet U_{crack,r} \bullet S_{crack} \sum_{k=1}^{Ncomp} f_2(C_k) \bullet \ddot{U}_k + \\ \frac{1}{r}\frac{\partial}{\partial \theta} U_{crack,\theta} \bullet S_{crack} \sum_{k=1}^{Ncomp} f_2(C_k) \bullet \ddot{U}_k \\ + \frac{\partial}{\partial z} U_{crack,z} \bullet S_{crack} \sum_{k=1}^{Ncomp} f_2(C_k) \bullet \ddot{U}_k \end{bmatrix}
$$

$$
+ (1-\varepsilon_p)(\lambda) \begin{bmatrix} \frac{1}{r}\frac{\partial\left(r \bullet U_{crack,r} \bullet \rho_{crack} \bullet \ddot{U}_{crck,p}\right)}{\partial r} + \frac{1}{r}\frac{\partial\left(U_{crack,\theta} \bullet \rho_{crack} \bullet \ddot{U}_{crack,p}\right)}{\partial \theta} \\ + \frac{\partial\left(U_{crack,z} \bullet \rho_{crack} \bullet \ddot{U}_{crack,p}\right)}{\partial z} \end{bmatrix}
$$

$$
+ \left[(1-\varepsilon_g)(1-\lambda) \rho_{FT} \sum_{l=1}^{N_{reac,FTt}} n_{k,l} \bullet \eta_{l,FT} \bullet r_{k,l,FT} \bullet \Delta H_{l,FT} \right]
$$

$$
+ \left[(1-\varepsilon_g)(\lambda) \rho_{crack} \sum_{l=1}^{N_{reac,crackt}} n_{k,l} \bullet \eta_{l,crack,p} \bullet r_{k,l,crack} \Delta H_{l,crack} \right]
$$

Task 5. Sensitivity Analysis of Parameter

Comsol Multiphysics 3.2 with the reaction engineering model was used for simulation using the model developed. Figure 4 shows a coarse grid created by the software to solve the differential equations. The figure is primarily for demonstration and finer grid was used for the actual simulations. Parameters such a superficial gas velocity, pressure, temperature, syngas composition and inerts were evaluated to observe the sensitivity of the change in conversion to a small change in these parameters. It is planned to evaluate the reactor parameters for their effect on FT conversions. Results on limited simulations show that superficial gas velocity is by far the most sensitive operating parameter followed by inerts in the range of parameters studied.

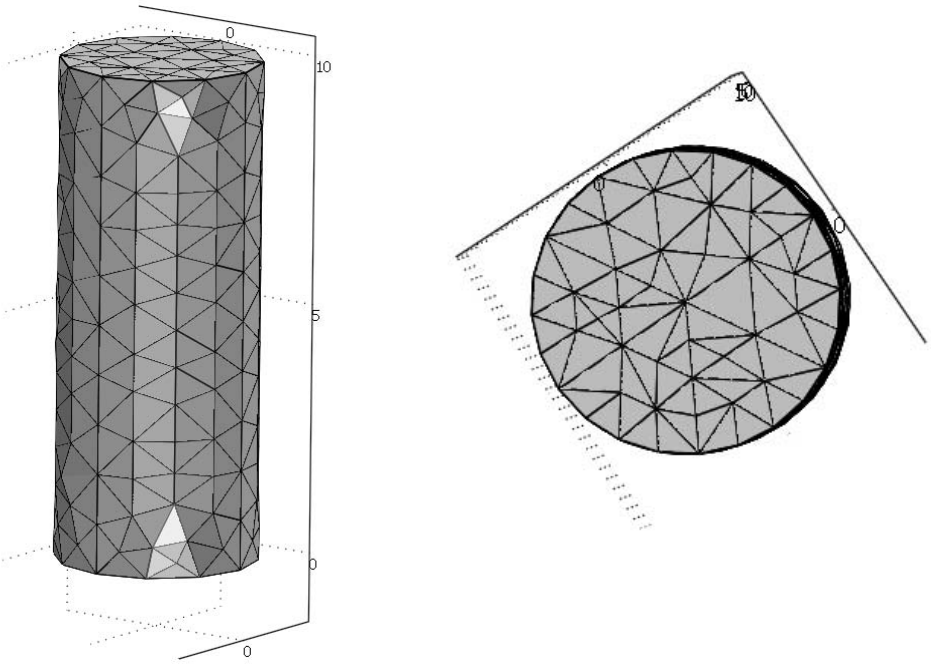

(a) side view (b) top view

Figure 4 Mesh setup of the reactor

Task 6. Model Validation, Prediction and Extension

The three most common regimes encountered during fluidization are bubbling, turbulent and fast fluidization. In dimensionless forms, the superficial fluid velocities are a function of Archimedes and Reynolds number. Based on the superficial velocities, the regime is determined. The developed model was then executed in Comsol Multiphysics 3.2 based on predetermined conditions and rate constants available in literature. For the sake of simplicity, the following assumptions were made:

1. The flow was assumed to be unidirectional - z- axis,
2. Axial dispersion was not neglected,

3. Convective gas and diffusion were equated to the product of the mass transfer coefficient and the concentration gradient across the element in each direction,
4. The effectiveness factor was assumed to be 1,
5. Catalyst deactivation was not considered,
6. Steady state operation was assumed.

The following show typical results in normalized forms obtained during such simulations. Figure 5 is a plot of CO conversion profile in the radial direction. It is observed that the conversions are highest at the edges and lowest at the center. However, the moles converted (not shown) shows a reverse trend. Figure 6 is a plot of the CO concentration as a function of height. As expected, the CO content decreases with height. Figure 7 shows the selectivity toward CO_2 generation at different bed heights while Figure 8 contains the distribution of hydrocarbons in the product.

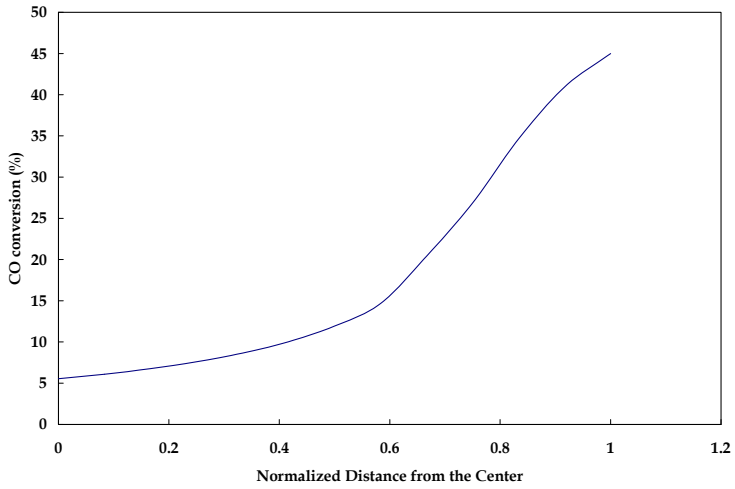

Figure 5. CO conversion as a function of radius at a given height

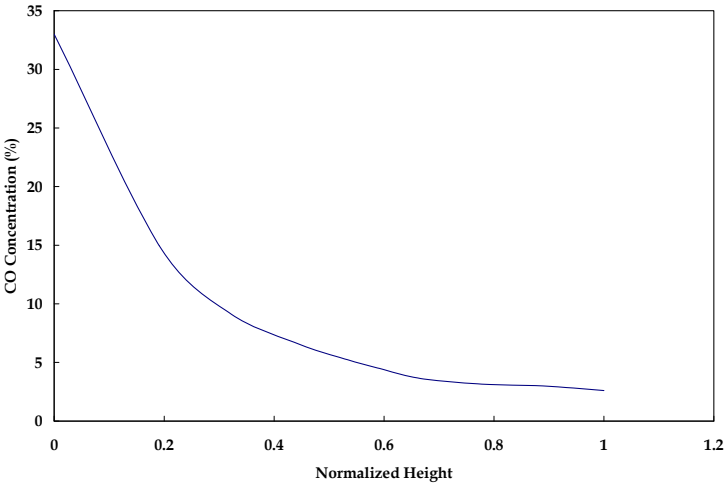

Figure 6. CO conversion as a function of height.

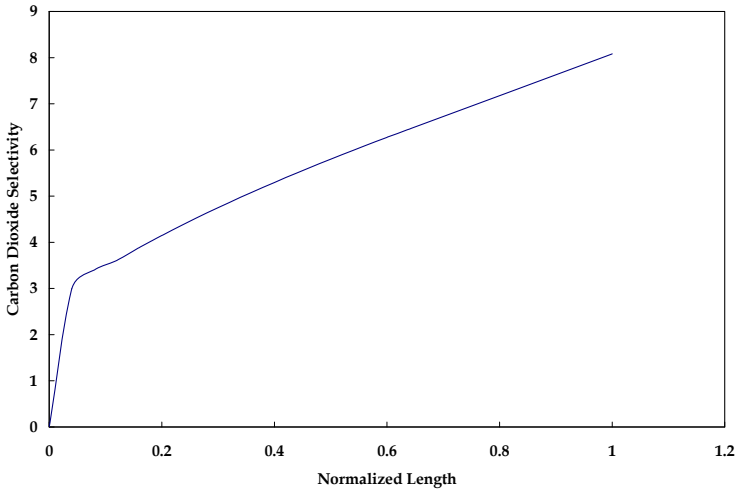

Figure 7. CO_2 selectivity as a function of height.

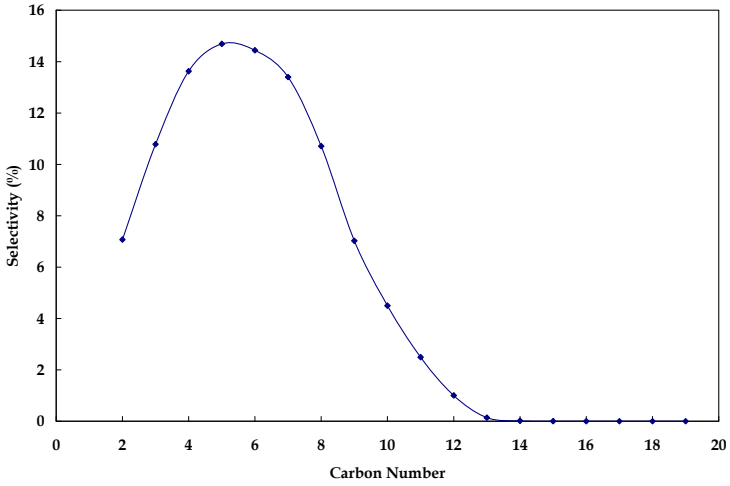

Figure 8. Product distribution/

CONCLUSIONS AND RECOMMENDATIONS

The following conclusions were made:

A generalized dynamic population balance model was developed.

Models were developed in both cartesian and cylindrical coordinates.

Both energy and mass balance were considered for developing temperature and concentration profiles.

Axial and lateral mixing of solids were considered.

Both, FT and cracking catalysts were included in the model.

Simplified version of the model was executed in the Comsol Multiphysics 3.2 software.

Based on the results and model development, the following recommendations are made.

The above model considered only one bed. In the case of dual bed formation, different zones based on physical considerations have to be segregated and separately modeled and then integrated. In addition, consideration for shocks at regime changeovers needs to be made.

The data available on the Texaco-Chevron studies should be extracted properly and then used extensively to validate the model.

Laboratory experiments should be designed in a small scale to extract model parameters.

REFERENCES

Linghu, W., Li, X., Fujimoto, K.; Supercritical Phase Fischer-Tropsch Synthesis Over Cobalt Catalyst", *Fuel Processing Technology*, 85 (8-10): 1121 -1138 (2004).

Hall, C.C.; "Recent Research On The Fischer-Tropsch Synthesis", *21st Congress of Industrial Chemistry*, Brussels, September, 1948, reprinted from *The Industrial Chemist*, (1949).

Demeter, J.J. and Schlesinger, M. D.; "Fischer-Tropsch Synthesis In Fluidized Catalyst Reactor With Nitrided, Fused-Iron Catalyst", United States Bureau of Mines, Report of Investigation 5456, (1959).

Texaco-Chevron Report on Fluidized Bed FT Synthesis, http://www.fischer-tropsch.org/primary_documents/industry_reports/Texaco%20Fluidized%20Bed%20Fischer-Tropsch%20Reports%20(courtesy%20of%20ChevronTexaco%20Corporation)/Texaco-Reports_toc.htm

DISCLAIMER STATEMENT

This report was prepared by Dr Kanchan Mondal, Southern Illinois University, Carbondale, with support, in part, by grants made possible by the Illinois Department of Commerce and Economic Opportunity through the Office of Coal Development and the Illinois Clean Coal Institute. Neither Dr. Kanchan Mondal, Southern Illinois University, nor any of its subcontractors, nor the Illinois Department of Commerce and Economic Opportunity, Office of Coal Development, the Illinois Clean Coal Institute, nor any person acting on behalf of either:

(A) Makes any warranty of representation, express or implied, with respect to the accuracy, completeness, or usefulness of the information contained in this report, or that the use of any information, apparatus, method, or process disclosed in this report may not infringe privately-owned rights; or

(B) Assumes any liabilities with respect to the use of, or for damages resulting from the use of, any information, apparatus, method or process disclosed in this report.

Reference herein to any specific commercial product, process, or service by trade name, trademark, manufacturer, or otherwise, does not necessarily constitute or imply its endorsement, recommendation, or favoring; nor do the views and opinions of authors expressed herein necessarily state or reflect those of the Illinois Department of Commerce and Economic Opportunity, Office of Coal Development, or the Illinois Clean Coal Institute.

Notice to Journalists and Publishers: If you borrow information from any part of this report, you must include a statement about the state of Illinois' support of the project.